ELSEVIER

Computer Physics Communications 143 (2002) 222–240

Computer Physics Communications

www.elsevier.com/locate/cpc

Numerical solving of the vibrational time-independent Schrödinger equation in one and two dimensions using the variational method

Jernej Stare, Janez Mavri *

National Institute of Chemistry, Hajdrihova 19, 1000 Ljubljana, Slovenia

Received 7 November 2001; accepted 19 November 2001

Abstract

A program package for variational solving of the time-independent Schrödinger equation (SE) in one and two dimensions is described. The first part of the the program package includes the fitting program (FIT) with which the *ab initio* or DFT calculated points are fitted to a computationally inexpensive functional form. Proper fitting of the potential energy surface is crucial for the quality of the results. The second part of the package consists of a program for variational solving of the SE (2DSCHRODINGER) using either a shifted Gaussian basis set or the rectangular basis set proposed by Balint-Kurti and coworkers [J. Chem. Phys. 91 (1989) 3571]. The third part of the program package consists of the calculation of the expectation values, IR and Raman spectra XPECT), and the visualization of results (PLOT). The program package is applied to study a quantum harmonic oscillator and an intramolecular, strong hydrogen bond in picolinic acid N-oxide. For the former system analytical solutions exist, while for the latter system a comparison with the experimental data is made. The advantages and disadvantages of the applied methods are discussed. © 2002 Published by Elsevier Science B.V.

PACS: 03.67.Lx; 31.15.-p; 31.15.Pf; 33.20.Tp

Keywords: Variational method; Schrödinger equation; Hydrogen bond; Vibrational spectroscopy; Rectangular basis set; Gaussian basis set

1. Introduction

Hydrogen bonding is essential for the structure and function of molecules, many of which are relevant in molecular biology. Small wonder, then, that a huge number of studies have been concerned with the structure and dynamics of hydrogen bonded systems [1–39]. For a recent work dealing with the theoretical treatments of hydrogen bonding see [40] and the references therein.

Hydrogen bonded systems are highly anharmonic and therefore their computational treatment in a harmonic approximation is of very limited value. On the other hand, rapid progress in advanced experimental techniques, such as the pulse-echo treatment of hydrogen bonding dynamics [41], require computational support that should, ideally, be state-resolved. The ideal solution would consist of numerical solving of the time-dependent Schrödinger equation (SE) for the nuclei. For a recent progress concerning solutions

* Corresponding author.
E-mail address: janez@kihp2.ki.si (J. Mavri).

0010-4655/02/$ – see front matter
PII: S0010-4655(01)00457-X

of the time-dependent Schrödinger equation see [42]. However, the currently available CPU power allows for solving the time-dependent SE for only twelve degrees of freedom. Time-independent SE provides solutions that are still of high value for the interpretation of experimental data; thus, they are useful for the interpretation of the vibrational spectra of hydrogen bonded systems.

Vibrational spectra contain complete information on the structure and electronic and nuclear dynamics of hydrogen bonds. Calculations of the vibrational spectra of hydrogen bonded systems are extremely demanding since their potential energy hypersurfaces are highly anharmonic; therefore, calculations of the vibrational spectra in the harmonic approximation are of very limited value.

In the past, a variety of methods have been developed for solving time-independent SE. They include: shooting methods that have been extended to more dimensions [30,43]; Anderson Monte Carlo [44]; genetic algorithms [45]; and variational methods [46–48]. In this article we deal with the variational solving of the SE.

The procedure for solving the vibrational time-independent Schrödinger equation consists of:

- calculation of the potential energy surface (PES) (*ab initio* or DFT calculations),
- fitting of the PES to an empirical form that allows for fast (preferably analytical) calculation of the matrix elements,
- calculation of the matrix elements,
- Hamiltonian matrix orthogonalization (if necessary),
- Hamiltonian matrix diagonalization,
- calculation of the observables and visualization of the results.

These steps are implemented in our program package. For the structure of the program package and flow of information see Fig. 1.

This article describes the methods implemented in the program package for variational solving of the one and two-dimensional Schrödinger equation using: (i) a grid basis set and (ii) displaced two-dimensional Gaussian basis functions. Solving the one-dimensional SE is much less demanding than solving the two-dimensional SE. Let us make a comparison between the one- and two-dimensional cases. If one considers twenty basis functions for the first dimension and twenty basis functions for the second dimension then in the one dimensional case one has to deal with a Hamiltonian matrix of 20×20, while in the two-dimensional case the Hamiltonian matrix is 400×400. Certain functional forms of the potential energy functions allow for analytical evaluation of the matrix elements. The choice of functional form for fitting of the hypersurface is therefore an important element in solving the SE. In this article CPU and memory requirements are thorougly examined.

The organization of this article is as follows: Section 2 describes the applied computational methods. Features of the model system (picolinic acid N-oxide, abbreviated PANO) and the details concerning the DFT calculations are given in Section 3. Computational performance of our program package is outlined and discussed in Section 4. The results obtained by applying our program package to the model system are summarized and discussed in Section 5. Concluding remarks and perspectives are given in Section 6.

2. Computational methods

For the flowchart depicting the flow of information in our program package see Fig. 1.

2.1. System Hamiltonian and the linear variational method

In order to calculate the anharmonic vibrational energy levels and the corresponding wavefunctions from the PES, one must solve the vibrational time-independent Schrödinger equation $\widehat{H}\Psi = E\Psi$, where $\widehat{H}$ consists of the kinetic part ($\widehat{T}$) and the potential part ($\widehat{V}$) ($\widehat{H} = \widehat{T} + \widehat{V}$). For an N-dimensional system in the internal coordinate representation, the kinetic and potential energy operators are defined as:

$$\begin{aligned} \widehat{T} &\equiv -\sum_{i=1}^{N} \frac{\hbar^2}{2\mu_i} \frac{\partial^2}{\partial s_i^2}, \\ \widehat{V} &\equiv V(s_1, \ldots s_N), \end{aligned} \tag{1}$$

where μ_i are the reduced masses and s_i are the internal coordinates. The potential energy function is typically determined from pointwise semi-empirical, *ab initio*, or DFT electron structure calculations.

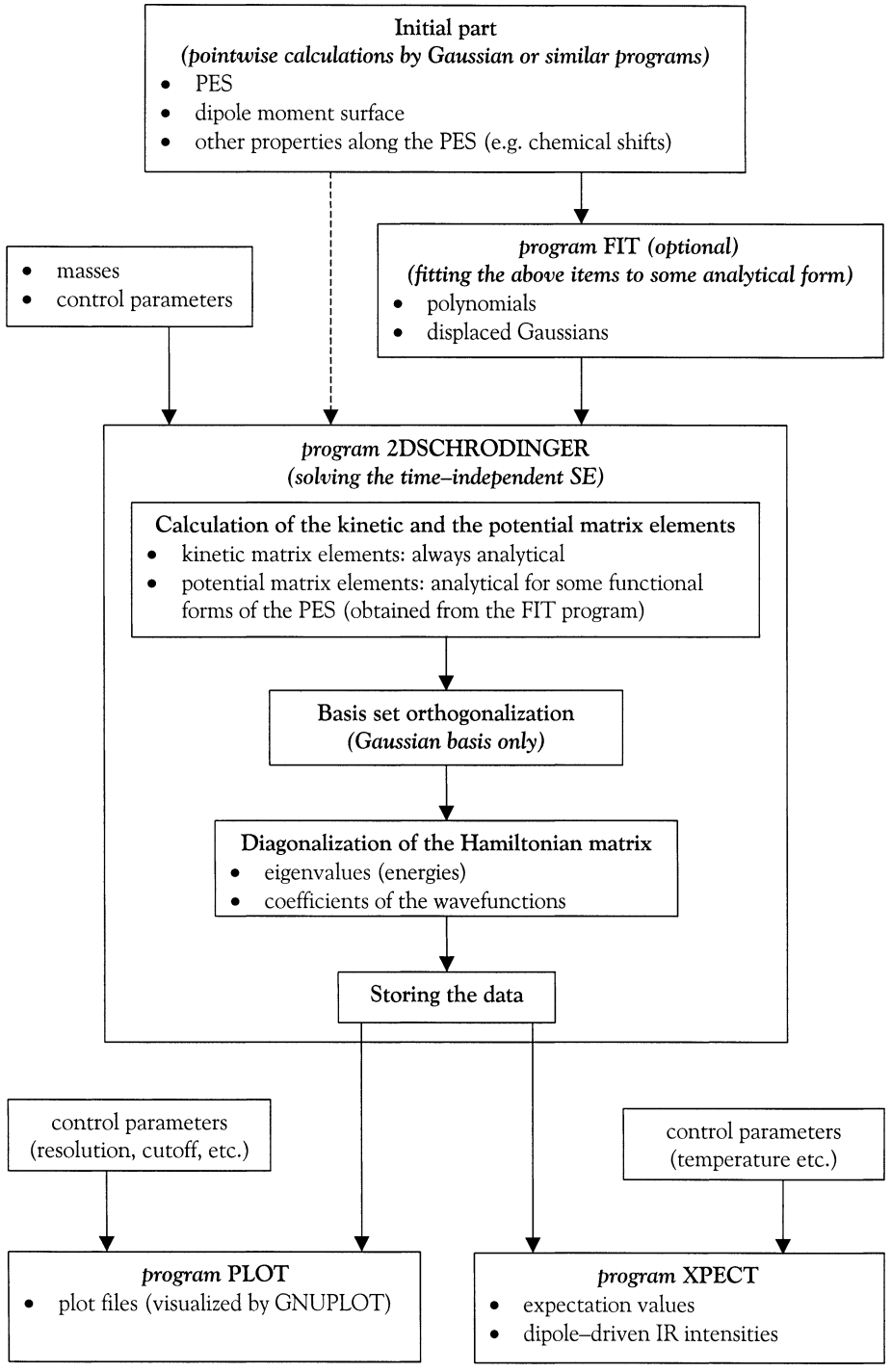

Fig. 1. Program package flowchart.

Of the various numerical techniques for solving the Schrödinger equation, the variational method is one of the most commonly used. Particularly useful is the linear variational method which is based on expressing the searched wavefunction Ψ as a linear combination of Nb normalized basis functions ϕ_i:

$$\Psi \equiv \sum_{i=1}^{Nb} c_i \phi_i, \tag{2}$$

where c_i are the corresponding coefficients which need to be determined. The system Hamiltonian is represented in the basis $|\phi_i\rangle$ as a $Nb \times Nb$ matrix **H** whose elements are H_{ij}. H_{ij} can be expressed as a sum of kinetic and potential contributions: $H_{ij} = T_{ij} + V_{ij}$. The Schrödinger equation then simplifies to a matrix equation

$$\mathbf{HC} = \mathbf{SCE}. \tag{3}$$

The overlap matrix **S** consists of overlap integrals.

If the basis is not orthogonal, it has to be orthogonalized prior to diagonalization. In our program two orthogonalization routines are implemented: symmetric and canonical [46].

2.2. Fitting the PES

It is not practical to calculate the matrix elements using CPU demanding *ab initio* or DFT calculation. It is highly recommended to fit the PES to the empirical form suitable for fast evaluation of the matrix elements.

Both the accuracy of the calculation and the CPU demands depend on the way the potential energy is expressed. Recall that the points on the PES can be calculated by *ab initio* or other electron structure determination methods. Thus, the PES is initially given by a set of points $V_i^0(x_i, y_i)$. We have implemented several approaches in fitting analytical functions to these points: cubic splines, polynomial fits, Gaussians, and an Empirical Valence Bond (EVB) approach.

The advantage of Bicubic Spline Fitting is that the function passes through all the given points, V_i^0, i.e. the interpolation is typically very good. The extrapolation, however, can cause significant troubles because of the potentially physically unrealistic behaviour of the fitted function beyond the range of the original points (x_i, y_i). There are two kinds of splines: gridded and scattered. In gridded splines the points are arranged in a rectangular grid, while scattered splines are not. However, the scattered spline approach is much more CPU time consuming. Since it is not usually easy to obtain the *ab initio* or DFT calculated regular grid we built in the possibility of transforming the scattered spline into the gridded spline at the beginning of the run.

In our program we considered fitting the hypersurface to some additional functional forms. We considered polynomial expansion, a set of two-dimensional shifted Gaussian functions, and the Empirical Valence Bond (EVB) form [49]. The latter method has become widely used in the computational treatment of enzymatic reactions, but the potential energy matrix elements are not analytical. We programmed the EVB functional form and tested it for two VB representations of the 1D proton potential. Unlike splines, the least-square interpolation can deviate from the given set of points V_i^0. This can lead to significant errors especially when the original points in the lower region of the hypersurface deviate from the fitted function. To avoid this, it is practical to weight (W_i) the points during the fitting procerdure according to the scheme $W_i \propto 1/(V_i^0 + K)$, where K is a constant. Such a functional form of the weighting scheme minimizes the errors. For PANO K values of 0.0001–0.1 kcal/mol were used (*vide infra*).

2.3. Vibrational basis sets

The choice of the basis set is essential for the variational solving of the Schrödinger equation. We tested two different basis sets: a grid basis set consisting of local constants, and displaced Gaussian functions basis set. With a linear combination of shifted Gaussians one can build Gauss–Hermite polynomials of the higher order. Since the Gauss–Hermite polynomials are eigenfunctions of the quantum harmonic oscillator, a small number of the Gaussian basis functions relative to the the grid basis functions will be required. The grid basis functions benefit from the fact that they are orthogonal and hence no orthogonalization is needed. For the Gaussian basis set we expect a smaller number of the basis functions.

The two-dimensional shifted Gaussians are characterized by four parameters: two coordinates of the center and two exponential constants, each in one direc-

tion. The normalization factor is determined from the exponential constants.

Optimization of the basis set is also very important. In the case of the grid basis set, one can vary the number of the basis functions and the span of the basis set. In the case of Gaussian basis functions, there are more parameters which can be varied. First of all, it is a good idea to choose a basis set of uniformly distributed Gaussians with the same spread, i.e. where all the values of the exponential constants α_i are the same. Next, the basis set range can be defined as for the grid basis set taking into account the spreads of the Gaussian functions. Assuming that the effective boundary of a Gaussian function is 3σ away from its center (note that $\sigma = 1/\sqrt{2\alpha}$), the effective basis set range thus begins at 3σ before the center of the first Gaussian and ends at 3σ after the last Gaussian. The most troublesome part of the optimization arises from the fact that the spacing between the Gaussians and their exponential parameter (α) depend on each other. For a given value of α, the spacing should be neither too small nor too large. Gaussians that are too far apart (large "gaps") obviously fail to describe the searched wavefunctions properly. If the Gaussians are too close, the neighbouring basis functions become almost identical to each other and are, thus, close to being linearly dependent. As a result, some eigenvalues of the overlap matrix essentially approach zero (due to numerical roundoffs, they can even assume very small negative values). Consequently, the symmetric orthogonalization procedure is useless in such cases. Canonical orthogonalization may be applied, resulting in a reduced number of solutions. Optimization of the Gaussian basis set is not trivial, and, more to the point, the orthogonalization procedure cannot be avoided. If a very large number of basis functions is required (e.g., if one is considering more than two dimensions), the procedure can be rationalized by using algorithms for finding only 10–100 of the lowest eigenvalues of the Hamiltonian rather than performing the full diagonalization. The grid basis set is clearly more promising in cases requiring a large number of basis functions.

2.4. Calculation of the matrix elements

Calculation of the matrix elements is associated with significant CPU effort when solving the Schrödinger equation using the variational method. It is not practical to perform several milion two-dimensional integrations numerically. The calculation of the overlap matrix elements takes advantage of the availability of analytical expressions using both implemented functional forms for the basis set. We have also implemented analytical expressions for the kinetic matrix elements in both bases. In contrast to the kinetic matrix elements, which can all be calculated analytically, the availability of analytical expression for the potential matrix elements depends on the functional form in which the potential energy function $V(x, y)$ is given. We used analytical expressions for the potential energy matrix elements where possible. For the rectangular grid basis set we calculated the potential energy matrix elements by numerical integration using the Gauss–Legendre quadrature. This is an extension of the original algorithm proposed by Balint-Kurti and coworkers [26,27], where the matrix elements are calculated by considering only the potential energy value above the center of the basis function. We demonstrated that the latter approximation is valid only for sufficiently fine grids. For PANO (*vide infra*) the 20×20 grid is already fine enough to allow such an approximation.

2.5. Diagonalization of the matrices

Matrix diagonalization is one of the most CPU-intensive procedures in the variational solving of the Schrödinger equation. When using the Gaussian basis set, the overlap matrix must also be diagonalized in order to orthogonalize the basis set using the canonical or symmetric procedure. In our program both Jacobi and Householder matrix diagonalization schemes have been implemented. Among various diagonalization routines, the Householder algorithm is the most favourable in terms of CPU time. It consists of a transformation of the initial matrix to a tridiagonal matrix which is diagonalized in the next step [50]. The Householder algorithm is also widely used in several *ab initio* and DFT program packages such as Gaussian 98.

2.6. Expectation values and IR intensities

The solution of the Schrödinger equation directly yields the energies and their corresponding wavefunctions. With these wavefunctions and eigenvalues we

can calculate the expectation values of all other quantities (metric parameters, NMR chemical shifts, etc.), as well as the dipole driven transition intensities, using the similarity tranformation [46]. The matrix elements can be analytically calculated for some functional forms, while for others numerical integration is required. In our program we implemented the same functional forms for the dipole moment as for the potential energy hypersurface. When calculating the IR intensities we considered the possibility of providing a dipole moment hypersurface in addition to the energy hypersurface. The IR spectrum is thus calculated beyond the limit of the electrical harmonicity. It is worth stressing that the Raman spectra can be calculated by replacing the dipole moment function by the corresponding polarizability function. When calculating observables corresponding to the finite temperature, the excited vibrational states were taken into account. Thermal averaging is performed analytically: excited states are considered using the corresponding Boltzmann weights.

2.7. Computational limits and hardware requirements

The number of points to be calculated to obtain the PES, as well as the number of basis functions, increases exponentially with the number of dimensions. Each dimension in the PES typically requires about 10 points, hence the number of calculations is of the order of 10^N for N dimensions. For a system of moderate size (e.g., picolinic acid N-oxide, $C_6H_5NO_3$), a reliable *ab initio* or DFT calculation (e.g., B3LYP/6-$31 + G(d, p)$ single point plus the forces) takes a few hours on a 700 MHz PC/Linux machine. The calculation of PES can therefore take several months if more than two dimensions are considered. The problem associated with matrix diagonalization is very similar. In order to manipulate such matrices, an appropriate amount of physical or swap memory needs to be adressed. Consider a 2500 by 2500 matrix which has to be diagonalized. The matrix contains 6.25 million double precision numbers. This corresponds to 50 megabytes of memory having to be booked. Increasing the size of the matrix by a factor of two or four brings us close to the memory limit available nowadays on a typical workstation. Bearing in mind that each dimension requires about 15 basis functions, it is clear that detailed analysis is limited to a small number of dimensions. Another limiting factor is the visualization. Only one- and two-dimensional potential surfaces and wavefunctions can be fully visualized and easily controlled. We do not want to say that higher dimensions are not possible to handle (we can always use the two-dimensional projections), but it is clear that such treatment is much more difficult and time consuming. While extention to more dimensions is methodologically straightforward and quite easy from the code developmend standpoint, it is computationally very demanding. Therefore, we remained with two-dimensional systems.

The program package for fitting the PES, calculating the matrix elements, solving the vibrational Schrödinger equation, calculating the expectation values and IR intensities, and visualization of the results was developed in our laboratory. The FORTRAN code, written in accordance with the FORTRAN-77 standards, was compiled with a GNU project g77 compiler. We avoided the calls of the system-dependent routines, which makes our program package easily portable to other platforms. The graphical output of the program is compatible with GNUPLOT [51], which is a public domain program for diagram plotting. The calculations were performed on a cluster of sixty-four PC/Linux machines based on an AMD Athlon processor at 700 MHz with 128 K on-die Level 1 and 512 K off-die Level 2 cache memory at $2/5$ of the processor clock frequency. There were 128 MB of physical memory (PC 100 SDRAM) and an additional 450 MB of swap memory installed on the hard disk. The overall disk space was 6.2 GB.

3. Model systems

The program 2DSCHRODINGER was developed and thoroughly tested on one- and two-dimensional harmonic oscillators. The advantage of these systems is that they allow for analytical evaluation of the eigenvalues and eigenfunctions. In this way all the parameters that are entering the variational calculation (the number of basis functions, functional form of the basis set, accuracy of the numerical integration, etc.) can be controlled. The results concerning the harmonic oscillators are not reported on here in the interests of space; we have concentrated rather on realistic systems.

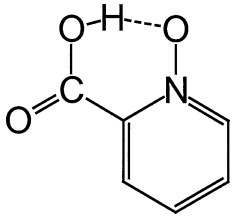

Fig. 2. The structure of picolinic acid N-oxide (PANO).

Picolinic acid N-oxide (PANO) (see Fig. 2) is an example of a strong hydrogen bond with an asymmetric single well proton potential. In crystalline PANO, the neutron diffraction determined O. . .O and the O–H distances are 2.428 and 1.091 Å, respectively [52]. The observed O–H stretching band in the infrared spectrum of the solution of PANO is located in the 1380–1450 cm^{-1} range, depending on the solvent [53]. The chemical shift of the proton participating in the intramolecular hydrogen bonding is about 18 ppm, indicating a strong hydrogen bond [54]. We have recently studied the dynamics of the hydrogen bond in PANO using quantum-dynamical methods with an included external electromagnetic field. A proposal for the IR-driven proton transfer was given [34].

Plain *ab initio* and DFT geometry optimizations seem to underestimate the strength of the hydrogen bond in PANO in terms of the metric parameters. The B3LYP/6-31 + G(d, p) calculated O. . .O distance in the optimized structure is 2.509 Å, which is considerably longer than the experimental value of 2.428 Å. Several other levels of theory give similar results for the metric parameters, which (in particular the O. . .O, O–H, and N–O distances) differ from the experimental values considerably. The O–H stretching frequency calculated in the harmonic approximation is 2965 cm^{-1}. Such discrepancies clearly indicate the anharmonicity of the O–H. . .O moiety and the necessity for its quantum treatment. An additional source of discrepancy between the calculated and measured metric parameters can be attributed to environment effects.

The two-dimensional potential energy surface of PANO was calculated pointwise along the O–H (x) and the O. . .O (y) distances on the B3LYP/6-31 + G(d, p) level. The range of the x- and y-values was chosen so that the minimum of the projections of the potential along both the x- and y-axis on the borders was at least 15 kcal/mol above the global minimum of the potential. We constructed a grid of 165 points corresponding to a rectangular grid of the O. . .O and O–H distances: 2.10, 2.20, 2.30, 2.35, 2.40, 2.45, 2.50, 2.55, 2.60, 2.65, 2.70, 2.80, 2.90, 3.00 and 3.20 Å (O. . .O); 0.80, 0.90, 1.00, 1.10, 1.20, 1.30, 1.40, 1.50, 1.60, 1.70 and 1.80 Å (O–H). Each point of the PES required about 4.5 hours of CPU time for the calculation on a 700 MHz PC/Linux machine. The calculations providing the PES were performed with the Gaussian-98 suite of programs [55]. In order to obtain a functional form of the PES suitable for analytical potential matrix elements, we fitted a 2D polynomial, as well as a set of Gaussian functions, to the original DFT pointwise calculations. We used a quasi-Newton minimization algorithm. The same procedure was applied to determine the dipole moment as a function of the O. . .O and O–H distances. We also considered the fit of the PES to the 2D polynomials. In the case of the 2D polynomial, all the coefficients in the expansion up to a specified degree were optimized. In the case of the 2D Gaussian functions, five parameters were subjected to optimization in each Gaussian: the normalization factor (a linear parameter), as well as the coordinates of the center and the exponential terms in both directions (nonlinear parameters). A constant term was added to the Gaussians to represent the hard core potential and also optimized. Several weighting schemes were applied to stress the importance of the points in the low energy regions. The fit quality was given by the average error (i.e. the difference between the original points and the fitted function) and by the distribution of the error over several energy regions. While an error of about 3 kcal/mol is of little importance to the fit quality at PES regions higher than 20 kcal/mol above the minimum, it plays a devastating role in the region just near the minimum. Tables 6 and 7 list the quality of fit for the PES and the dipole moment function of PANO. Fig. 3 displays the PES fitting error as a function of the energy for two distinct fitting schemes.

4. Computational performance

4.1. Matrix operations

The economics of matrix diagonalization is an important issue since this is one of the most CPU-intensive parts of the program. Table 1 shows the effi-

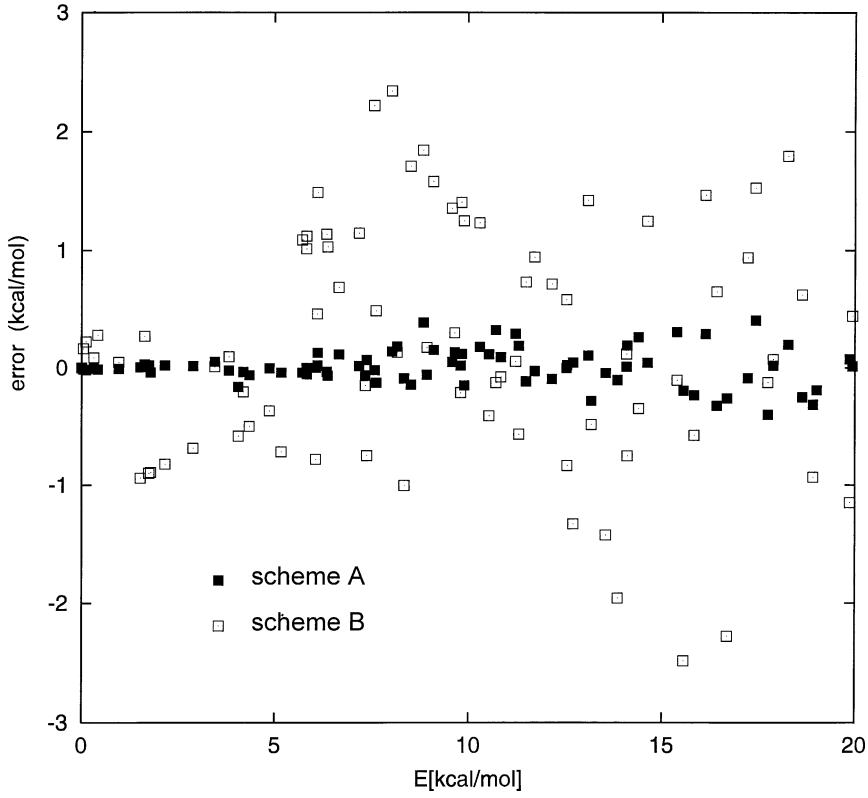

Fig. 3. The distribution of error for the points in the lowest energy region ($E \leqslant 20$ kcal/mol) for two fitting schemes of the potential energy function of PANO (referred to as A and B in Table 8).

Table 1
Average CPU time (in seconds) for diagonalization of overlap matrices of several sizes ($Nb \times Nb$)

Nb	100	200	300	400	500	625	750	1000	1600	2000	2500
Jacobi	1.0	9.2	37.5	104.6	204.5	465.1	782.7	1972.0	4348.8	18,673.4	41,716.8
Householder	0.2	1.5	5.4	13.3	26.0	52.7	91.3	220.0	680.8	1776.5	3590.9

ciency of two distinct diagonalization routines in terms of the CPU time. It is clear that the Householder reduction to a triagonal matrix followed by diagonalization is superior to the Jacobi rotation algorithm. Table 1 shows that the CPU time required for the matrix diagonalization is third-power dependent on the size of the matrix.

It is worth stressing that the CPU time needed for diagonalization strongly depends not only on the size of the matrix, but also on the arrangement of its elements. Namely, a matrix that is already close to the diagonal form will take much less time to be diagonalized than a less ordered matrix. In this sense, it is obvious that the diagonalization involved in basis set orthogonalization (the highly ordered overlap matrix ressembling a block-diagonal one) is faster than the diagonalization of the Hamiltonian matrix. In addition, the Hamiltonian matrix represented in the grid basis takes less time to be diagonalized because the potential energy contributions are zero for the off-diagonal elements.

Like the matrix diagonalization, the CPU time for the matrix multiplication is also third-power with respect to the matrix size and represents a significant part of the overall CPU time. This makes symmetric orthogonalization (2 multiplications) less favourable

Table 2
The required memory for the program to run as a function of the maximum number of basis functions (Nb)

Nb	100	289	400	484	625	729	1024	1600	2000	2500	3600
Memory (MB)	12.4	16.9	21.5	26.1	35.6	44.2	75.8	168.1	262.2	393.4	803.1

Table 3
The CPU time for the calculation of potential matrix elements (analytical integration) for several degrees of the polynomial potential energy surface. The basis set consists of 676 Gaussian functions, i.e. $Nb_x = Nb_y = 26$

$\mathrm{Deg}_x/\mathrm{Deg}_y$	2/2	4/2	4/4	6/2	6/4	6/6	8/2	8/4	8/6	8/8
Time (seconds)	4.07	8.17	15.16	13.42	25.00	39.72	20.01	36.62	57.38	82.82

with respect to the canonical orthogonalization (1 multiplication). Although both yield the same results, canonical orthogonalization is preferable since it not only saves CPU time but also avoids problems where there is a linear dependence in the basis set. The difference in CPU times between the symmetric and canonical orthogonalization simply corresponds to the matrix multiplication (see row H′ in Table 5) for a given basis set size. In contrast to the diagonalization, the CPU demands for the multiplication do not depend on the arrangement of the elements.

4.2. Memory

Table 2 lists the amount of memory that should be requested in order for the program to run several maximum matrix sizes. The 2D arrays where the matrices are stored require the most memory. Note that the listed amount of memory is more a formal than a real demand. When the program runs, the peak memory usage is well below the requested amount. However, if less memory (dynamic + swap) is available than requested, the program will not run properly. A 3600 by 3600 matrix (corresponding to a two-dimensional basis set of 60×60 basis functions) is close to, or even beyond, the upper limit of available memory on a typical workstation.

4.3. The functional form of the potential

The potential energy matrix elements are analytical if the PES is described by a polynomial expansion or by Gaussian functions. Thus, the degrees of the polynomial representing the PES have an impact on the calculation performance. The same is true for the number of Gaussian functions in the Gaussian-fitted PES. The influence of these parameters on performance is shown in Tables 3 and 4 for a system of a medium size (26 by $26 = 676$ basis functions). Both tables reproduce the linear dependence of the CPU time on the total number of coefficients (polynomial PES) or on the number of Gaussians (Gaussian PES).

Table 4
The CPU time for the calculation of potential matrix elements for different numbers of the Gaussians representing the PES. The basis set consists of 676 Gaussian functions, i.e. $Nb_x = Nb_y = 26$

Ng	1	3	5	10	15	20	30	50	100
Time (seconds)	0.90	1.29	1.83	2.81	3.83	4.87	7.43	11.65	22.69

4.4. Overall performance of the program in solving the Schrödinger equation

Table 5 lists the required CPU times for the grid, as well as the Gaussian basis sets and for various basis set sizes. The potential matrix elements were obtained using an analytical expression for the integrals. If the numerical integration were applied instead, it would be by far the most time consuming part of the program. Therefore, the grid basis approach is far more economic than the Gaussian basis, mostly due to orthogonalization. The Gaussian basis approach can yield more reliable results for 2D harmonic systems and needs fewer basis functions, however, this advantage vanishes in the case of realistic, strongly anharmonic potentials.

Table 5
CPU times (in seconds) for various routines of the program using the 2D model polynomial PES of the second degree

$Nb_x \times Nb_y$	10×10	16×16	20×20	26×26	30×30	34×34	40×40	50×50
Nb	100	256	400	676	900	1156	1600	2500
				Gaussian basis				
O	0.0	0.8	4.3	23.4	60.8	126.9	343.3	1503.3
T	0.0	0.0	0.1	0.3	0.4	0.7	1.5	4.1
V	0.1	0.6	1.4	4.0	7.4	11.7	22.5	55.6
H′	0.0	1.1	10.4	84.4	198.4	461.6	1427.5	7138.0
D	0.0	1.4	9.8	64.3	161.7	380.7	1081.8	5307.1
S	0.1	0.8	1.8	5.2	12.2	23.0	44.0	118.8
Total	0.3	4.7	28.9	182.0	441.8	1006.2	2924.5	14,152.0
				Grid basis				
T	0.0	0.0	0.1	0.3	0.6	0.8	1.9	4.0
V	0.0	0.0	0.0	0.1	0.3	0.3	0.9	1.7
D	0.0	0.8	4.2	24.3	63.9	145.4	411.1	1709.4
S	0.1	0.8	1.8	5.5	12.4	23.9	46.4	107.1
Total	0.2	1.7	6.4	30.6	77.2	165.6	458.1	1854.7

O—orthogonalization; T—calculation of kinetic matrix elements; V—calculation of potential matrix elements; H′—calculation of the Hamiltonian matrix in an orthogonal base; D—diagonalization of the Hamiltonian matrix; S—storing the data. Note that the potential matrix elements have been calculated analytically.

4.5. Performance of the program for calculation of the expectation values

The CPU demands for calculations of the expectation values and the IR intensities were found to be very much dependent on the type of basis set. For the grid basis, the calculation is very fast (it takes, in most cases, less than 1 second to calculate of the following items (no matter what the size of the basis set is): (a) expectation values of the coordinates x and y, (b) a property represented by a $6/6$ polynomial for 10 distinct eigenstates, and (c) the relative IR transition intensities between all possible pairs of these states. For the Gaussian basis set, the calculation is much more CPU-demanding. The impact of the basis set size and the representation of the dipole moment or some optional property (e.g., the degrees of the polynomial) is much more pronounced in the case of the Gaussian basis set. The calculation of one expectation value of a variable represented by a $6/6$ polynomial along the PES, the wavefunction being represented by a 30×30 Gaussian basis set, takes about 150 seconds. About the same time is required for one IR intensity if the dipole moment function is represented as a $6/6$ polynomial. A calculation usually includes about 10 expectation values and 45 intensities. It may take more than 8000 seconds to complete the calculations for a typical system, compared with about 1000 seconds (see Table 5) needed to solve the Schrödinger equation. The extraction of expectation values may therefore take much more CPU time than the calculation of the eigenfunctions.

5. Results and discussion

As stated in the introduction, we will only report the results for PANO. This is a strongly anharmonic system. The applied computational parameters should also be applicable, with minor changes, to other hydrogen-bonded systems.

5.1. Basis set optimization

In order to get a satisfactory number of reliably calculated eigenvalues and eigenfunctions, we first set the effective range of the functions constituting the basis set for PANO. The range was between 0.70 and 2.10 Å in the O–H direction and between 2.05 and 3.35 Å in the O…O direction. We set the mass associated with the O–H mode yo 1 amu and that with the O…O mode to 20 amu. This reproduces both the experimental frequency corresponding to this mode in the 250–300 cm^{-1} region and the calculated value

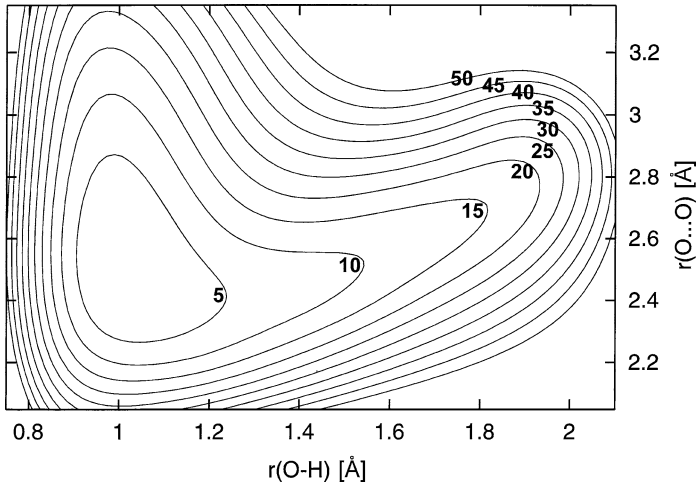

Fig. 4. Potential energy surface for PANO. The energy values (relative to the minimum) pertaining to the contours are given in kcal/mol.

of 276 cm^{-1} (in the harmonic approximation) fairly well [53].

Having set the ranges of the coordinates, we explored the convergence of the results as a function of the parameters of the basis functions. We found the Gaussian basis set to be troublesome, since the optimal exponential parameters α obtained from the harmonic approximation were much too small to yield good results. As a result, we used the grid basis throughout.

First, we solved the Schrödinger equation with a very large basis set (60×60 basis functions). The so obtained eigenvalues and $1 \rightarrow N$ frequencies were set as a reference. Next, we applied various smaller basis sets and compared the resulting frequencies with the reference results. We define the "error" of a particular basis set in the ith frequency as the difference between the calculated ith frequency obtained by the basis set of interest and the 60×60 basis set. The error increases with increasing vibrational level. For basis sets with sizes close to the reference (60×60), the error was smaller. In the range of interest (we chose 30–50 of the lowest levels), there was a relatively small error with basis sets of small or moderate size (see Fig. 5). For PANO, the grid basis set of 20 basis functions in the O–H direction and 36 in the O...O direction is the smallest basis set that yields satisfactory enough results. We found that an incomplete basis set in one direction (e.g., 14×20) also has an impact on the energies of the excited states in the other direction (see Fig. 6).

Knowing the reference eigenvalues allowed us to optimize the Gaussian basis functions. The optimized values of the exponential parameters of the vibrational basis functions for PANO in the above-mentioned ranges should be 20 kcal/(mol Å)^2 in the O–H direction and 58 kcal/(mol Å)^2 in the O...O direction. The optimal values in our system, however, turned to be 50 and 200 kcal/(mol Å)^2, respectively. The number of Gaussian functions required to achieve the same precision relative to a very big basis set was nearly the same as in the case of the grid basis set. The main advantage of the Gaussian basis set over the grid, i.e. that it provides the same precision with fewer basis functions and is valid in a harmonic system, vanishes in this system.

5.2. Frequencies, expectation values and IR intensities

Different fitting schemes for the PES yield different results in terms of eigenvalues and wavefunctions. The quality of fit strongly affects the calculated $1 \rightarrow N$ frequencies, but only influences wavefunctions to a minor extent.

Table 8 lists certain frequencies obtained by solving the vibrational Schrödinger equation for PANO with a grid basis set containing 20 basis functions along the O–H direction and 36 along the O...O direction, for a total of 720 basis functions. The spline fitting scheme is added as a reference since the interpolated PES

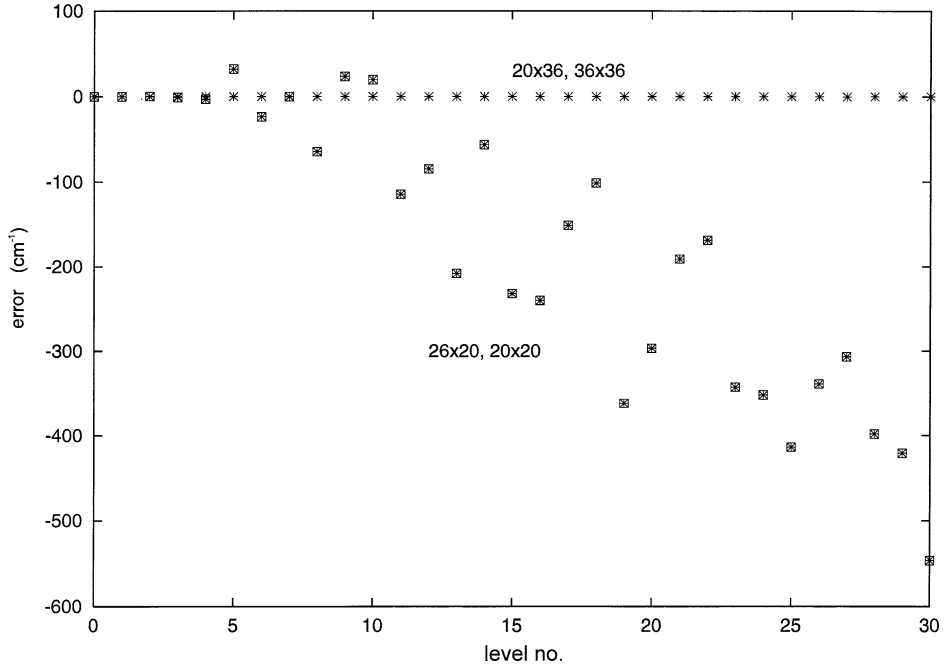

Fig. 5. Error (i.e. the difference between the frequencies of PANO obtained by a given basis set and the frequencies obtained by a large 60×60 grid basis set) for four distinct grid basis sets: 36×36, 20×36, 36×20 and 20×20, for the first 30 vibrational levels.

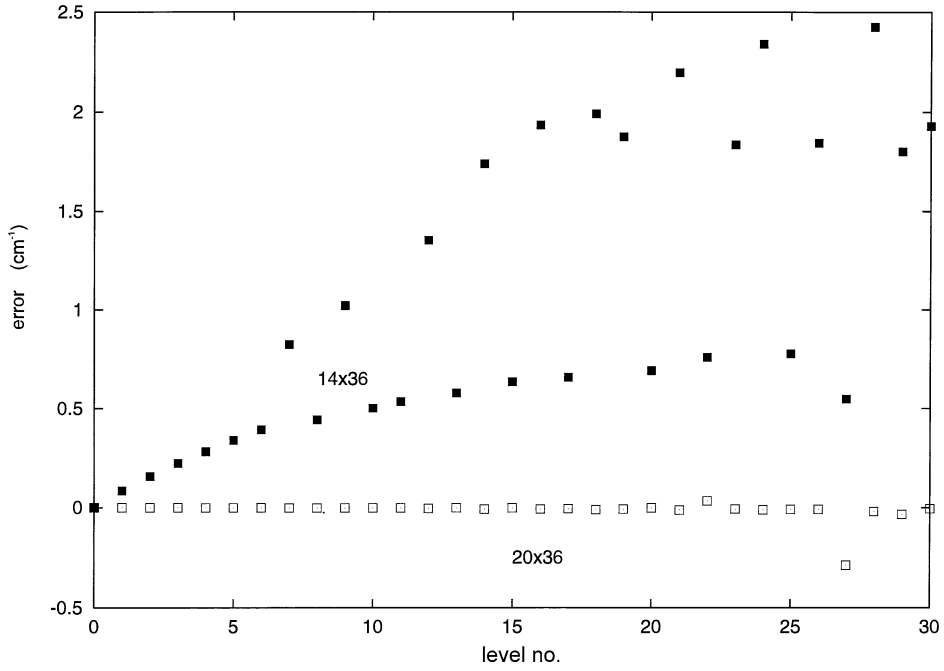

Fig. 6. Error for a 20×36 and a 14×36 grid basis set for the first 30 vibrational levels of PANO.

Table 6
The fitting quality of an analytical functions to a pointwise calculated PES (B3LYP/6-31 + G(d, p) calculations)

Label	A	B	C
Type of fit	11 Gaussians	4/4 polynomial	8/4 polynomial
N_{add}	0	1	1
$\langle\text{error}\rangle_{\text{total}}$	0.1594	1.1392	0.5126
$\langle\text{error}\rangle_1$	0.0110	0.1330	0.0200
$\langle\text{error}\rangle_5$	0.0301	0.3925	0.0815
$\langle\text{error}\rangle_{10}$	0.0657	0.7695	0.3219
$\langle\text{error}\rangle_{20}$	0.1117	0.8416	0.3619

N_{add} corresponds to the number of additional points needed to achieve proper asymptotic behaviour of the fitted function. $\langle\text{error}\rangle_x$ corresponds to average absolute error (in kcal/mol) in the energy region between 0 and x kcal/mol.

Table 7
The quality of fitting analytical functions to a pointwise calculated dipole moment

Label	M_A	M_B
Type of fit	linear	5/5 polynomial
$\langle\text{error}\rangle$	0.2889	0.0220

$\langle\text{error}\rangle$ corresponds to average absolute error (in Debyes).

Table 8
Some fundamental vibrational frequencies of PANO (in cm^{-1}) for the different fitting schemes listed in Table 6 and for the spline-fitted PES. The initial state is always the ground state. The final state is labelled according to the excitation in the O–H/O...O direction. "0" represents the ground state, "1" first excited, and so on. For example, the label "1/2" denotes the level with the first excited state in O–H and second excited state in the O...O mode. A grid basis set of 20×36 functions was used throughout (see text for details)

Final state	A	B	C	Splines
0/1	278.15	306.93	295.85	282.22
0/2	554.12	604.41	583.58	554.66
0/3	827.57	892.77	863.87	828.10
1/0	1732.96	2018.76	1749.90	1723.18
1/1	2138.48	2384.59	2135.38	2116.53
1/2	2526.03	2742.21	2513.05	2492.45
2/0	2945.56	3212.59	2993.08	2926.46

Table 9
The effect of isotopic substitution of H-bonded hydrogen in PANO on the O–H and O...O stretching frequencies

Undeuterated		Deuterated		$\nu_{\text{OH}}/\nu_{\text{OD}}$
ν_{OH}	ν_{OO}	ν_{OD}	ν_{OO}	
1732.96	278.15	1421.38	266.19	1.219

passes through all the initial points. The worst fit (B) gives significantly different frequencies than the other schemes and is therefore not applicable. In particular, the best fitting scheme (A) yields frequencies very similar to the spline-fitted PES. The deviations are larger for the states with higher excitations of the O–H and/or O...O modes.

The isotopic substitution (i.e. the H-bonded proton replaced by deuterium) changes both the eigenvalues and the wavefunctions. Typically, the O–D stretching frequencies are red-shifted. The effect of the isotopic substitution can be readily calculated by inserting the mass of 2 amu when solving the Schrödinger equation. In Table 9 gives a comparison of the O–H and O...O stretching frequencies of both unsubstituted and deuterium-substituted PANOs.

The expectation values of the O–H and O...O distances calculated using the thermally averaged expectation values is a quantum corrected optimized geometry of the O–H...O moiety. For low temperatures it is enough to include only about 5–10 of the lowest levels in the Boltzmann averaging (for safety, we used the 20 lowest levels in our calculations). Table 10 lists the expectation values for the O–H and O...O distances for various levels and in both environments. Thermal averages of the distances are calculated at 15 and 295 K since neutron diffraction determined structures are available at these temperatures. The plain B3LYP/6-31 + G(d, p) optimized distances are added for comparison. The quantum correction for the O–H and the O...O modes considerably shifts the calculated metric parameters towards the experimental values. The calculated O...O distance shrinks from 2.5088 to 2.4786 Å (15 K) when the quantum correction is taken into account.

The temperature dependence of the O–H and O...O distances, which is due to the changes in the level population, is noteworthy. The decrease in r_{OH} on changing the temperature from 15 to 295 K indicates that the excited O...O states with lower values of $\langle r_{\text{OH}}\rangle$ are more populated. The calculated decrease in r_{OH} with increasing temperature is in agreement with the experiment, although it is less pronounced.

Expectation values are also affected by isotopic substitution. We observed that on replacing the H-bonded proton by deuterium, the expectation values for the O–H distance decreased and the O...O distance increased. This phenomenon is referred to as Ubbe-

Table 10
Expectation values of the O–H ($\langle r_{OH}\rangle$) and the O...O ($\langle r_{OO}\rangle$) distances (in Å) in PANO for the ground state and certain excited states (see Table 8 for explanation of the labeling of the levels). Boltzmann-averaged expectation values of these distances over the first 20 levels at two distinct temperatures (15 and 298 K); the B3LYP/6-31 + G(d, p) optimized distances and the experimental (neutron scattering at 15 and 295 K) distances are also listed. The vibrational Schrödinger equation was solved by a 20×36 grid basis set with the PES given by fitting scheme A (see Table 6)

Level	$\langle r_{OH}\rangle$	$\langle r_{OO}\rangle$
0/0	1.0621	2.4786
0/1	1.0582	2.4956
1/0	1.2170	2.4491
1/1	1.2042	2.4585
avg. (15 K)	1.0621	2.4786
avg. (295 K)	1.0609	2.4846
B3LYP/6-31 + G(d, p) geometry optimization	1.0115	2.5088
neutron diffraction (15 K)	1.091	2.428
neutron diffraction (295 K)	1.069	2.428

lohde effect [39,56]. The X-ray crystal structures for both undeuterated and deuterated PANO at 125 K are available. The calculated elongation of the O...O distance is in good agreement with experimental observations. The calculated and experimental distances are listed in Table 11.

Lastly, the relative dipole-driven IR transition intensities were calculated for the O–H...O moiety in PANO using various dipole moment functions, temperatures, and isotopes. Since no dynamic information is available and there is no coupling to the rest of the environment, the usual band broadening does not appear; such a spectrum should be represented as a linear combination of delta functions $\sum_i \delta(\omega - \omega_i)$. In order to obtain more realistic spectra, we also plotted the bands as Lorenzians with a constant half-width of 100 cm^{-1}.

We found electrical anharmonicity to have a profound impact on the pattern of the intensities. Fig. 7 shows a comparison between the spectra of the O–H...O moiety in PANO calculated by approximating the electric harmonicity (dipole moment function fitting scheme M_A, Table 7) and by the inclusion of electric anharmonicity (dipole moment function fitting scheme M_B). The inclusion of electric anharmonicity

Table 11
Thermally averaged expectation values (at 125 K, in Å) of the O–H and the O...O distance in both the undeuterated and deuterated PANO. The X-ray determined O...O distance at 125 K is also listed. Details on solving the vibrational Schrödinger equation are given with Table 10

		Undeuterated	Deuterated
Calculated	r_{OH}	1.0620	1.0437
	r_{OO}	2.4793	2.4903
X-ray	r_{OO}	2.434	2.446

causes a 4-fold relative increase in the O–H stretching intensity and in the intensities of transitions involving O–H excited states (relative to the O...O stretching intensity). It can be seen from the fitting schemes (Table 7) that the electrical harmonic approximation fails to reproduce the behaviour of the dipole moment function. Therefore, it is important to take into account electric anharmonicity when calculating the spectra.

With increasing temperature, the population of the excited states also increases and, consequently, more bands corresponding to the transitions from the excited states appear. The hot transitions appear in the spectrum. Fig. 8 displays the spectra of the O–H...O moiety in PANO calculated at 15 and 298 K. The appearance of additional bands leads to the effective broadening of the O–H stretching band. This band was also found to be very broad in our experiments [53]. It is worth reemphasizing that we did not take into account the coupling of the O–H...O moiety to the rest of the environment and we did not consider dynamic effects. Therefore, the calculated spectrum does not allow for quantitative comparison with the experiment.

Finally, the effect of isotopic substitution on spectra was studied. Apart from the frequency shifts (see Table 9), there is a 1.60-fold decrease in the O–H stretching intensity upon substitution of the H-bonded hydrogen by deuterium. The effects of deuteration on the spectrum of the O–H...O moiety in PANO is displayed in Fig. 9.

6. Conclusions

We have developed a program package for solving the vibrational Schrödinger equation in one and two

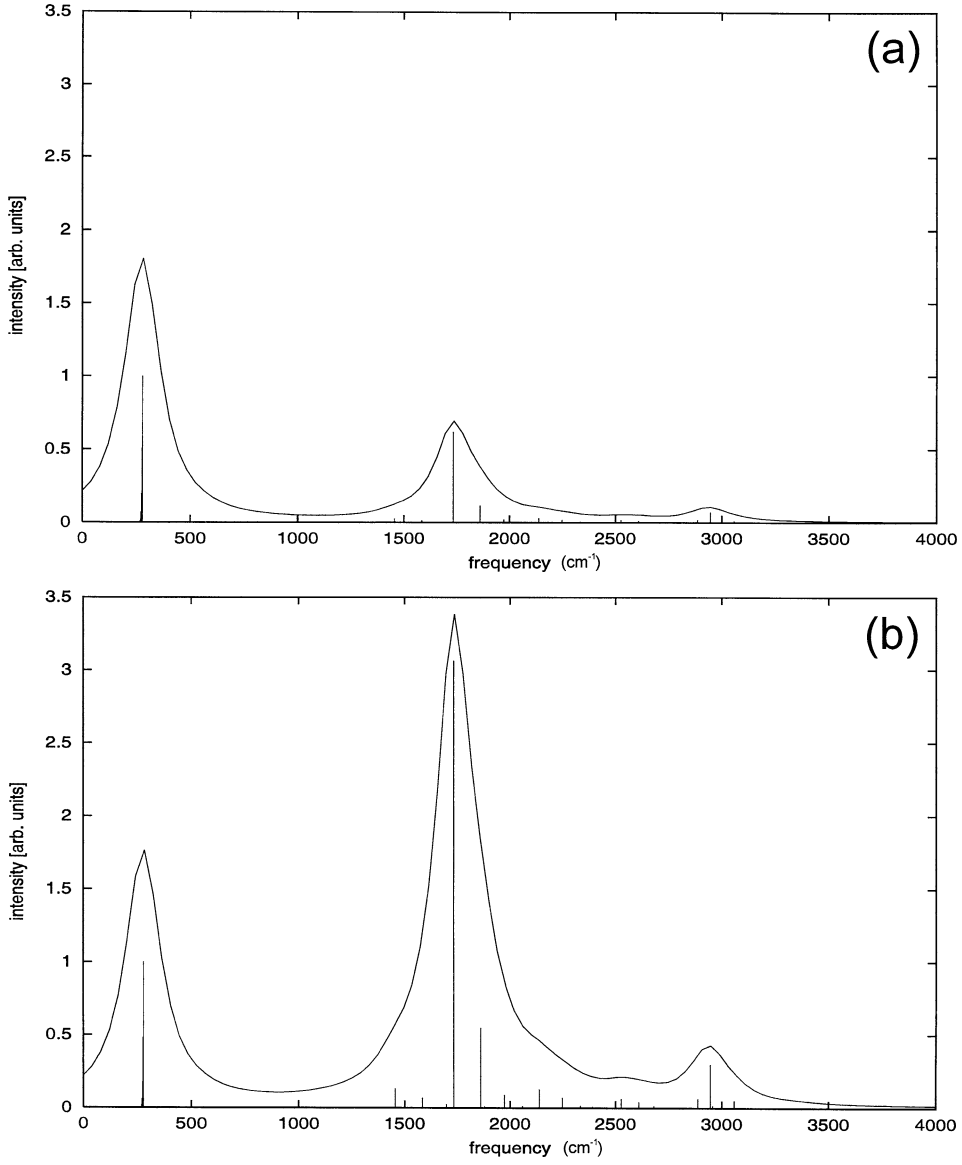

Fig. 7. Infrared bands of the O–H. . . O moiety in PANO at 298 K: (a) in an approximation of electric harmonicity (fitting scheme M_A in Table 7); (b) for the dipole moment represented by a 5/5 polynomial (fitting scheme M_B in Table 7).

dimensions. *Ab-initio* or DFT calculated potential energy surfaces are fitted to various functional forms that include: polynomial expansion, linear combination of Gaussians, splines, and an Empirical Valence Bond form. Proper fitting of the potential energy surface is essential for the calculated eigenvalues and eigenfunctions. For a strong hydrogen bonded system we found satisfactory representation of the 2D PES by a superposition of 11 shifted Gaussians. As basis functions we applied either shifted Gaussians or local constants on a rectangular grid. The vibrational Schrödinger equation was solved by a variational method. As a criterion for reliability we applied a given number of eigenvalues below the energy threshold that remain constant even if the size of the basis set is increased. We performed several test runs on harmonic oscillators

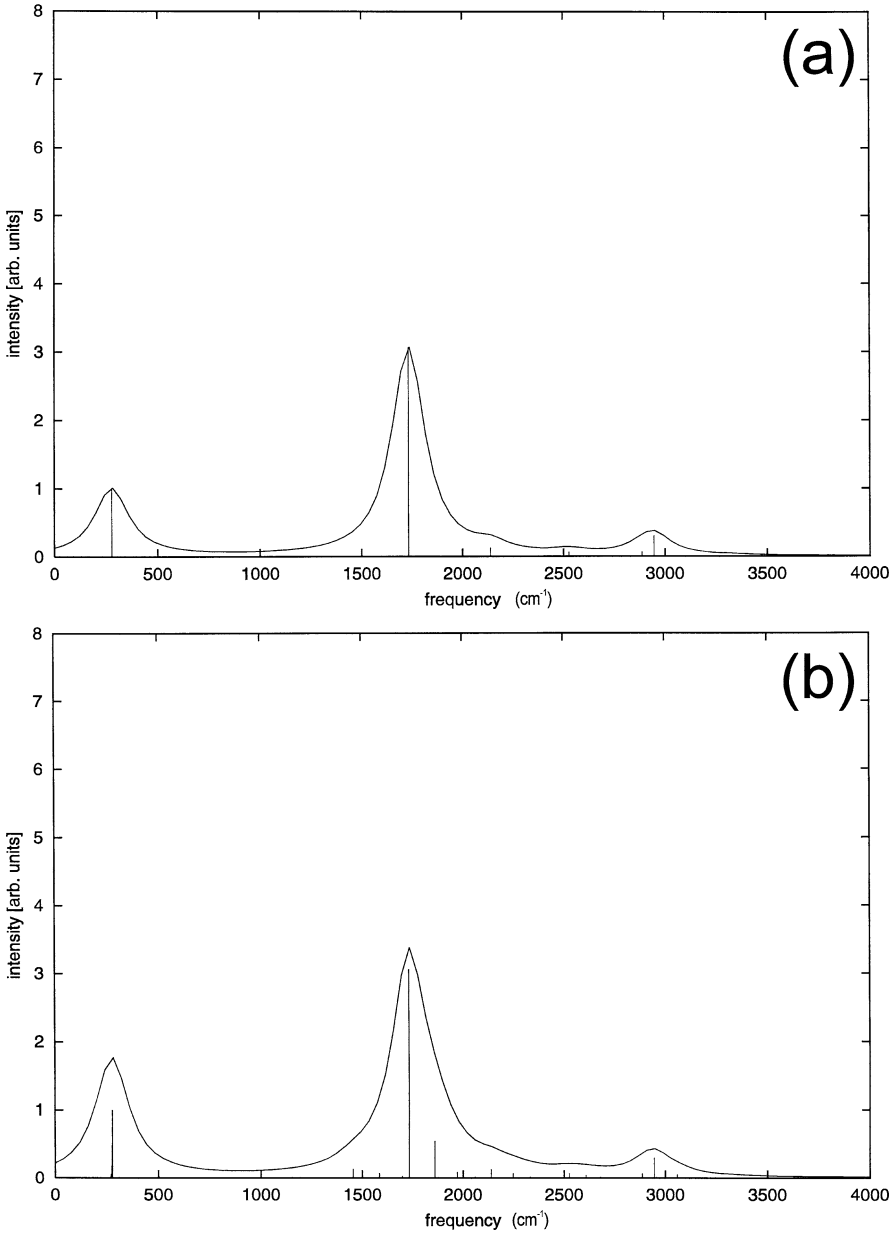

Fig. 8. Infrared bands of the O–H. . .O moiety in PANO: (a) at 15 K; (b) at 298 K.

and on the intramolecular strong hydrogen bond in picolinic acid N-oxide (PANO). Only for the harmonic systems is the Gaussian basis set more favourable than the grid basis in terms of CPU time and memory. We have demonstrated that the grid basis set has several advantages over the Gaussian basis set for realistic, anharmonic systems:

- The potential part of the Hamiltonian matrix is diagonal. This becomes important if the potential energy matrix elements are not analytical.
- For sufficiently fine grids, the integration of the potential energy matrix elements can be approximated by the potential function above the center of the basis function.

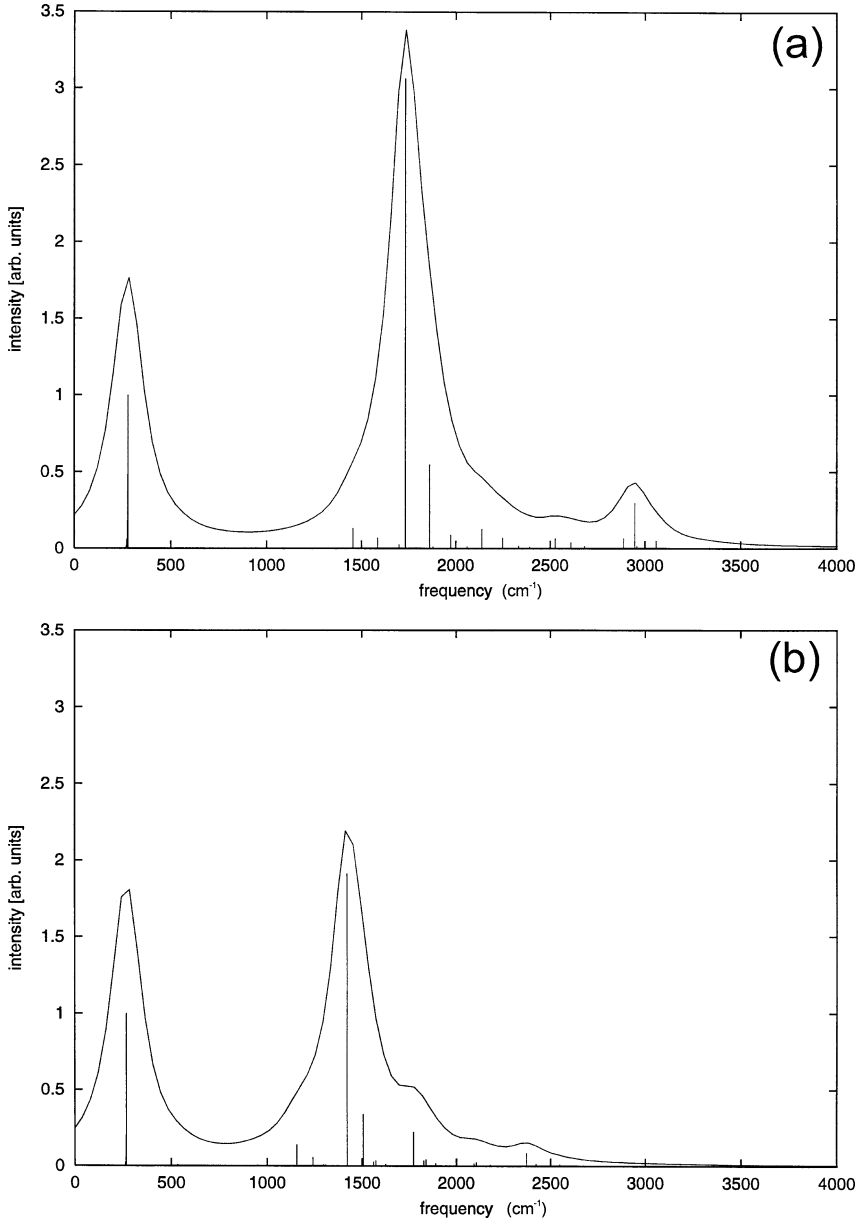

Fig. 9. Infrared bands of the O–H. . .O moiety in PANO at 298 K: (a) undeuterated; (b) deuterated.

- The grid basis set requires no orthogonalization. On the other hand, canonical orthogonalization with the Gaussian basis set requires overlap matrix diagonalization and one matrix multiplication.
- The grid basis set procedure is much easier to code.
- In the spirit of multidimensional problems, the grid basis set is more suitable for matrix diagonalization procedures that yield only a desired number of the lowest eigenvalues.

In the near future we hope to extend our approach to three and more dimensions. For the hydrogen bonded

systems the additional degrees of freedom that require quantum treatment include the in-plane O–H bending and carbonyl stretching. In addition, we will solve the problem of assignment of the masses via the G-matrix approach and the inclusion of kinetic coupling terms in Eq. (1). Moreover, we will introduce the possibility of hypersurface representation in the functional form of Molecular Mechanics for Chemical Reactions [57].

The code of the program package written in FORTRAN-77 can be obtained free of charge from one of the authors (J.S.) upon request (e-mail: jernej@hp14.cmm.ki.si).

Acknowledgements

Financial support from the Ministry of Science and Technology of the Republic of Slovenia is gratefully acknowledged. The authors would like to thank Prof. Dušan Hadži, National Institute of Chemistry, Ljubljana, Slovenia, and Nađa Došlić, Ruđer Bošković Institute, Zagreb, Croatia, for many stimulating discussions. Warm thanks are due to Dr. Thomas Steiner, Freie Universität, Berlin, Germany, for providing the X-ray and neutron diffraction data prior to their publication, and Prof. Zdzisław Latajka, University of Wrocław, Poland, for his critical reading of the manuscript. We are grateful to Ms. Charlotte Taft for linguistic corrections.

References

[1] B.J. Gertner, J.T. Hynes, Science 271 (1996) 1563–1566.
[2] K. Ando, J.T. Hynes, J. Phys. Chem. A 103 (1999) 10 398–10 408.
[3] D. Zahn, J. Brickman, Israel J. Chem. 39 (1999) 469–482.
[4] H. Azzouz, D. Borgis, J. Mol. Liquids 63 (1995) 89.
[5] H. Decornez, K. Drukker, S. Hammes-Schiffer, J. Phys. Chem. A 103 (1999) 2891–2898.
[6] J. Mavri, H.J.C. Berendsen, J. Phys. Chem. 99 (1995) 12 711–12 717.
[7] A. Fedorowitz, J. Mavri, P. Bala, A. Koll, Chem. Phys. Lett. 289 (1998) 457–462.
[8] S. Billeter, W. van Gunsteren, Comput. Phys. Comm. 107 (1997) 61–91.
[9] S. Billeter, W. van Gunsteren, J. Phys. Chem. A 104 (2000) 3276–3286.
[10] L. Jaroszewski, B. Lesying, J.A. McCammon, J. Mol. Struct. 283 (1993) 57–62.
[11] A. Tachibana, T. Inoue, M. Nagaoka, T. Yamabe, J. Phys. Chem. 93 (1989) 220–225.
[12] W. Klopper, M. Quack, M.A. Suhm, Chem. Phys. Lett. 261 (1996) 35–44.
[13] C.F. Guerra, F.M. Bickelhaupt, J.G. Snijders, E.J. Baerends, Chem. Eur. J. 5 (1999) 3581–3594.
[14] L. Jaroszewski, B. Lesyng, Chem. Phys. Lett. 175 (1990) 282–288.
[15] H.-H. Bueker, T. Helgaker, K. Ruud, E. Uggerud, J. Phys. Chem. 100 (1996) 15 388–15 392.
[16] A.J. Abkowicz-Bienko, Z. Latajka, J. Phys. Chem. A 104 (2000) 1004–1008.
[17] M. Fores, M. Duran, M. Sola, L. Adamowicz, J. Comp. Chem. 21 (2000) 257–269.
[18] C. Mijoule, M. Allavena, J.M. Leclercq, Y. Bouteiller, Chem. Phys. 109 (1986) 207–213.
[19] J.E.D. Bene, M.J.T. Jordan, Int. Rev. Phys. Chem. 18 (1999) 119–162.
[20] J. Laane, Int. Rev. Phys. Chem. 18 (1999) 301–341.
[21] S. Geppert, A. Rabold, G. Zundel, J. Phys. Chem. 99 (1995) 12 220–12 224.
[22] Y. Bouteiller, Z. Latajka, J. Chem. Phys. 97 (1992) 145–149.
[23] M. Eckert, J. Comp. Phys. 82 (1989) 147–160.
[24] G.M. Chaban, J.O. Jung, R.B. Gerber, J. Phys. Chem. A 104 (2000) 2772–2779.
[25] V. Alexandrov, D.M.A. Smith, H. Rostkowska, M.J. Nowak, L. Adamowicz, W. McCharty, J. Chem. Phys. 108 (1998) 9685–9693.
[26] G.G. Balint-Kurti, R.N. Dixon, C.C. Marston, Int. Rev. Phys. Chem. 11 (1992) 317–344.
[27] C.C. Marston, G.G. Balint-Kurti, J. Chem. Phys. 91 (1989) 3571–3576.
[28] J. Almlöf, Chem. Phys. Lett. 17 (1972) 49–52.
[29] B. Kuhn, T.R. Rizzo, D. Luckhaus, M. Quack, M.A. Suhm, J. Chem. Phys. 111 (1999) 2565–2587.
[30] M.V. Vener, O. Kühn, J. Sauer, J. Chem. Phys. 114 (2001) 240–249.
[31] N. Doslić, O. Kühn, J. Manz, Ber. Bunsenges. Phys. Chem. 102 (1998) 292–297.
[32] N. Doslić, O. Kühn, J. Manz, K. Sunderman, J. Phys. Chem. A 102 (1998) 9645–9650.
[33] N. Doslić, K. Sunderman, L. Gonzalez, O. Mo, O. Kühn, Phys. Chem. Chem. Phys. 1 (1999) 1249–1257.
[34] N. Doslić, J. Stare, J. Mavri, Chem. Phys. 269 (2001) 59–73.
[35] J. Mavri, J. Grdadolnik, J. Phys. Chem. A 105 (2001) 2039–2044.
[36] J. Mavri, J. Grdadolnik, J. Phys. Chem. A 105 (2001) 2045–2051.
[37] W. Siebrand, Z. Smedarchina, M.Z. Zgierski, A. Fernández-Ramos, Int. Rev. Phys. Chem. 18 (1999) 5–41.
[38] S. Scheiner, J. Phys. Chem. A 104 (2000) 5898–5909.
[39] M. Ichikawa, J. Mol. Struct. 552 (2000) 63–70.
[40] D. Hadži, Theoretical Treatments of Hydrogen Bonding, Wiley, 1997.
[41] S. Bratos, G.M. Gale, G. Gallot, F. Hache, N. Lascoux, J.C. Leickman, Phys. Rev. E 61 (2000) 5211–5217.
[42] M.H. Beck, A. Jäckle, G.A. Worth, H.-D. Meyer, Phys. Reports 324 (2000) 1–105.
[43] M.V. Vener, N.D. Sokolov, Chem. Phys. Lett. 264 (1997) 429–434.

[44] J.B. Anderson, J. Chem. Phys. 63 (1975) 1499–1503.
[45] D.E. Makarov, H. Metiu, J. Phys. Chem. A 104 (2000) 8540–8545.
[46] A. Szabo, N.S. Ostlund, Modern Qunatum Chemistry, MacMillan, 1982.
[47] D.J. Locker, J. Phys. Chem. 75 (1971) 1756.
[48] B.W. Shore, J. Chem. Phys. 59 (1973) 6450.
[49] A. Warshel, Computer Modelling of Chemical Reactions in Enzymes and Solutions, John Wiley and Sons, New York, 1991.
[50] W.H. Press, S.A. Teukolsky, W.T. Vetterling, B.P. Flannery, Numerical Recipes, Cambridge University Press, 1992.
[51] T. Williams, C. Kelley, GNUPLOT: A command driven interactive function plotting program, Department of Computer Science, Dartmouth College, Hanover, NH, 03755.
[52] T. Steiner, A.M.M. Schreurs, M. Lutz, J. Kroon, Acta Cryst. C 56 (2000) 577–579.
[53] J. Stare, J. Mavri, G. Ambrožič, D. Hadži, J. Mol. Struct. (THEOCHEM) 500 (2000) 429–440.
[54] B. Brzezinski, M. Szafran, Org. Magn. Reson. 15 (1981) 78–82.
[55] M.J. Frisch, G.W. Trucks, H.B. Schlegel, G.E. Scuseria, M.A. Robb, J.R. Cheeseman, V.G. Zakrzewski, J.J.A. Montgomery, R.E. Stratmann, J.C. Burant, S. Dapprich, J.M. Millam, A.D. Daniels, K.N. Kudin, M.C. Strain, O. Farkas, J. Tomasi, V. Barone, M. Cossi, R. Cammi, B. Mennucci, C. Pomelli, C. Adamo, S. Clifford, J. Ochterski, G.A. Petersson, P.Y. Ayala, Q. Cui, K. Morokuma, D.K. Malick, A.D. Rabuck, K. Raghavachari, J.B. Foresman, J. Cioslowski, J.V. Ortiz, B.B. Stefanov, G. Liu, A. Liashenko, P. Piskorz, I. Komaromi, R. Gomperts, R.L. Martin, D.J. Fox, T. Keith, M.A. Al-Laham, C.Y. Peng, A. Nanayakkara, C. Gonzalez, M. Challacombe, P.M.W. Gill, B. Johnson, W. Chen, M.W. Wong, J.L. Andres, C. Gonzalez, M. Head-Gordon, E.S. Replogle, J.A. Pople, Gaussian 98, Revision A.5, Gaussian, Inc., Pittsburgh, PA, 1998.
[56] J.M. Robertson, A.R. Ubbelohde, Proc. Roy. Soc. A 170 (1939) 222–241.
[57] T.V. Albu, J.C. Corchado, D.G. Truhlar, J. Phys. Chem. A 105 (2001) 8465–8487.